NMR structure and dynamics of the agonist dynorphin peptide bound to the human kappa opioid receptor

Casey O'Connor[a,b], Kate L. White[a,b,c], Nathalie Doncescu[d], Tatiana Didenko[a], Bryan L. Roth[c], Georges Czaplicki[d], Raymond C. Stevens[a,b,1], Kurt Wüthrich[a,e,f,1], and Alain Milon[a,d,1]

[a]Department of Integrative Structural and Computational Biology, The Scripps Research Institute, La Jolla, CA 92037; [b]Departments of Biological Sciences and Chemistry, Bridge Institute, University of Southern California, Los Angeles, CA 90089; [c]Department of Pharmacology, University of North Carolina Chapel Hill Medical School, Chapel Hill, NC 27514; [d]Institute of Pharmacology and Structural Biology, CNRS and Université de Toulouse-Paul Sabatier, 31077 Toulouse, France; [e]Department of Molecular Biology and Biophysics, ETH Zurich, CH-8093 Zurich, Switzerland; and [f]The Skaggs Institute for Chemical Biology, The Scripps Research Institute, La Jolla, CA 92037

Edited by Michael F. Summers, Howard Hughes Medical Institute, University of Maryland, Baltimore County, Baltimore, MD, and accepted by the Editorial Board August 13, 2015 (received for review June 2, 2015)

The structure of the dynorphin (1–13) peptide (dynorphin) bound to the human kappa opioid receptor (KOR) has been determined by liquid-state NMR spectroscopy. ^{1}H and ^{15}N chemical shift variations indicated that free and bound peptide is in fast exchange in solutions containing 1 mM dynorphin and 0.01 mM KOR. Radioligand binding indicated an intermediate-affinity interaction, with a K_d of ∼200 nM. Transferred nuclear Overhauser enhancement spectroscopy was used to determine the structure of bound dynorphin. The N-terminal opioid signature, YGGF, was observed to be flexibly disordered, the central part of the peptide from L5 to R9 to form a helical turn, and the C-terminal segment from P10 to K13 to be flexibly disordered in this intermediate-affinity bound state. Combining molecular modeling with NMR provided an initial framework for understanding multistep activation of a G protein-coupled receptor by its cognate peptide ligand.

GPCR activation | transferred NOE | ^{15}N relaxation | molecular dynamics simulations | ligand binding affinity

G protein-coupled receptors (GPCRs) are the largest superfamily of membrane proteins in the human genome and play a critical role in human physiology by initiating signal transduction in response to extracellular stimuli (1, 2). Since 2007, 89 GPCR crystal structures have been reported, including receptors in inactive and active states, as well as the beta-2 adrenergic receptor (β_2-AR) bound to heterotrimeric G proteins (3). NMR spectroscopy has revealed that the intrinsic conformational heterogeneity of GPCRs is influenced by ligand pharmacology, membrane composition, and effector interactions (4–6). These structural biology studies have provided atomic-resolution insights of systems defined by dynamic structural rearrangements that are correlated with diverse cellular and physiological outcomes.

The classic opioid receptors (δ/κ/μ) are GPCRs activated in response to binding enkephalin-like peptide agonists and are the primary targets of widely prescribed pain medications (7). The kappa opioid receptor (KOR) and its cognate peptide dynorphin are implicated in neuronal pathways associated with addiction, pain, reward, mood, cognition, and perception (8, 9). Nonselective KOR antagonists such as naltrexone have been prescribed for alcohol dependence with limited efficacy in humans, and next-generation KOR antagonists continue to be developed to treat drug addiction and other disorders. Although much is known regarding the antagonist-bound, inactive state of GPCRs, including the crystal structure of JDTic-bound KOR, the interaction of these receptors with neuropeptide agonists remains largely unknown (10). Peptide agonist-bound structures have thus far been limited to a conformationally stabilized neurotensin receptor, likely corresponding to a low-energy peptide-receptor state (11–13).

Dynorphin was discovered by Goldstein and Chavkin as the endogenous activating neuropeptide for KOR, with a "low-resolution" structural model of interaction proposed to PNAS in 1981 (14, 15). Dynorphins are derived from the precursor prodynorphin, with dynorphin A(1–17), dynorphin B(1–13), and alpha neoendorphin sharing a highly conserved N-terminal sequence and charge distribution (16). Dynorphin A(1–13) was shown to act as an agonist on opioid kappa receptors in vivo (17). Physiological activation of KOR is mainly associated with unwanted effects such as dysphoria, anhedonia, and hallucinations, and a current hypothesis in the field is that KOR functionally selective ligands may produce analgesia without dysphoria (18, 19). Functional selectivity has emerged as the leading model to understand the ability of a ligand to activate a subset of signaling cascades, providing a framework for developing next-generation drugs with rationally designed pharmacological profiles (20).

The seminal work of Schwyzer in the 1970s and 1980s led to a model of KOR activation by dynorphin that proceeds via a multistep binding mechanism (14, 21, 22). Thereby, low- to intermediate-affinity binding states of dynorphin correspond to binding to cell-surface membranes or to extracellular loops of the GPCR. A "message–address" paradigm has been formulated based on structure–activity relations observed with dynorphin analogs (21–26). Accordingly, the N-terminal YGGF "message" sequence, which is common to all opioid peptides, was found to be responsible for receptor activation. A C-terminal "address" sequence was further found to contribute via electrostatically driven interactions to KOR subtype specificity. In the context of this paradigm, the present study yields intriguing data on the N-terminal

Significance

The human kappa opioid receptor (KOR) is implicated in addiction, pain, reward, mood, cognition, and perception. Activation of KOR by the neuropeptide dynorphin is critical in mediating analgesia and tolerance. Our solution NMR study of dynorphin (1–13) provided quantitative data on a KOR-bound conformation. Analysis of the peptide structure and dynamics revealed a central helical turn bounded on both sides by flexibly disordered peptide segments. Future drug development will benefit from knowledge of the dynorphin structure bound to its human receptor.

Author contributions: R.C.S., K.W., and A.M. designed research; C.O., K.L.W., T.D., G.C., and A.M. performed research; C.O., K.L.W., N.D., T.D., B.L.R., and G.C. contributed new reagents/analytic tools; C.O., G.C., R.C.S., K.W., and A.M. analyzed data; and C.O., T.D., B.L.R., G.C., R.C.S., K.W., and A.M. wrote the paper.

The authors declare no conflict of interest.

This article is a PNAS Direct Submission. M.F.S. is a guest editor invited by the Editorial Board.

Data deposition: NMR, atomic coordinates, chemical shifts, and restraints have been deposited in the Protein Data Bank, www.pdb.org (PDB ID code 2N2F) and in the BioMagResBank, www.bmrb.wisc.edu (accession no. 25597).

[1]To whom correspondence may be addressed. Email: stevens@usc.edu, wuthrich@scripps.edu, or alain.milon@ipbs.fr.

This article contains supporting information online at www.pnas.org/lookup/suppl/doi:10.1073/pnas.1510117112/-/DCSupplemental.

segment of the KOR-bound opioid peptide dynorphin. The methods used, NMR in solution and molecular dynamics simulations, enabled us to define structural ensembles of KOR-bound dynorphin and to characterize internal peptide motions in the presently prepared low-affinity receptor-bound state.

Results

We prepared KOR with the approach used to solve the crystal structure in complex with JDTic by X-ray crystallography (10). The membrane fraction of *Spodoptera frugiperda* cells transiently expressing KOR was isolated and radioligand binding assays performed to assess receptor function. Dynorphin binding affinity was determined as ~200 nM at pH 7.4 and 6.1, consistent with an intermediate-affinity interaction (Fig. S1*A*). Following reconstitution of the receptor in detergent micelles and purification to >95% homogeneity, similar binding was measured and the preparation was stable at 7 °C for over a week (Fig. S1*B*). The following observations, made in the absence of G protein, thus characterize an intermediate state of KOR along its activation pathway, similar to what was recently described by ^{13}C-NMR for β_2-AR (27).

The dynorphin (1–13) peptide, YGGFLRRIRPKLK, was ^{15}N-labeled at residues G2, G3, F4, L5, R6, R7, I8, R9, and L12. [^{15}N, ^{1}H]-heteronuclear single quantum correlation (HSQC) NMR spectra of ^{15}N-(GFLIR)-dynorphin at pH 6.1 and pH 7.4 indicated the peptide adopts a random coil conformation in aqueous solution. Owing to little dependence of binding on pH, measurements were made at pH 6.1 to reduce proton exchange with solvent. Resonance assignments were obtained with 2D [^{1}H, ^{1}H]-total correlation spectroscopy (TOCSY) and nuclear Overhauser effect spectroscopy (NOESY), 2D [^{15}N, ^{1}H]-HSQC, [^{13}C, ^{1}H]-HSQC, and 3D CBCANH experiments, using standard pulse sequences and a classical ^{1}H assignment strategy for small peptides (28). ^{1}H, ^{13}C, and ^{15}N resonance assignments were deposited to the Biological Magnetic Resonance Data Bank (BMRB; accession no. 25597) (29).

Detergent-reconstituted KOR was added to an aqueous solution of dynorphin at a ratio of 1:100, with a 1 mM final concentration of peptide. KOR-specific binding of dynorphin was reversed by the addition of the high-affinity ligand JDTic at a molar ratio of 1:1 with respect to dynorphin. We thus isolated by difference analysis the nonspecific binding of dynorphin to the mixed detergent-sterol micelle of dodecyl maltoside/cholesteryl hemisuccinate (DDM/CHS). NMR-derived values such as chemical shift, NOE intensity, and relaxation rate constants (R_1, R_2, and ^{1}H-^{15}N NOEs) were obtained with and without JDTic to characterize a KOR-bound conformation of dynorphin.

Chemical Shift Perturbations. KOR-binding produced distinct patterns of dynorphin ^{1}H, ^{15}N, and ^{13}C chemical shift changes detected in 1D proton and 2D heteronuclear correlation NMR experiments, as shown in Fig. 1. The observation of chemical shift changes shows that the exchange rate between KOR-bound and KOR-unbound states is fast on the millisecond time scale, as the frequency difference between bound and unbound state is on the order of 10^3 Hz (Fig. 1*C*; see *Supporting Information* for further considerations on exchange rates). The sequence-specific changes were largest from L5 to R9, with smaller changes observed from G2 to F4 and K11 to K13. ^{15}N-^{1}H correlation experiments acquired without proton decoupling in the in-phase/anti-phase method (HSQC-IPAP) were obtained to determine $^{1}J_{NH}$ (30). No significant variations on the ^{15}N-^{1}H couplings was observed in HSQC-IPAP experiments, consistent with negligible residual dipolar couplings, and therefore anisotropic interactions do not contribute to the observed phenomena. The shifts observed on ^{1}H and ^{15}N are too large to be accounted for by secondary structure alone and likely reflect a ring current effect due to the receptor proximity. We measured the ^{13}C chemical shifts of C′, C^{α}, and C^{β} of ^{13}C-labeled arginine residues (R6, R7, and R9), because these values report on secondary structure (31). Based on carbon chemical shifts, a helical conformation was expected for R6 and R7, in contrast to R9. In addition to JDTic competition, the inhibition of dynorphin-specific binding was also observed using the highly potent KOR agonist ICI-199,441 (32). The observations and analysis performed here therefore describe a property of KOR–dynorphin-specific interaction reversible by agonists and antagonists.

Nuclear Overhauser Effects and Structure Determination. Where ligand exchange between a bound and free state is considered fast ($k_{off} > R_1$), transferred NOEs (trNOEs) originating from the receptor-bound state may be observed on the free peptide spectrum. The measured ^{1}H R_1 values for amide protons in the free state depended on the residue and ranged from 1.2 to 1.8 s^{-1} (Fig. S2). As expected from simulations (Fig. S3), our measurements confirm the dominant contribution of unbound dynorphin on R_1. When $k_{off} > \sigma_{ij}$, the cross-relaxation rate σ_{ij} is

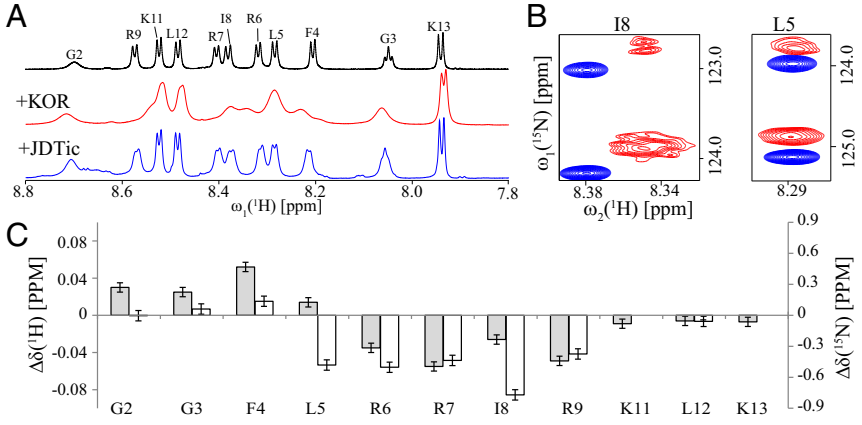

Fig. 1. Influence of KOR and JDTic on NMR spectra of dynorphin. (*A*) (top, black) 1D ^{1}H-NMR expansion of the NH region of dynorphin in aqueous solution at pH 6.1 acquired at 280 K. (middle, red) Addition of DDM/CHS reconstituted KOR induces significant line broadening for all resonances. The least broadened resonances were K11, L12, and K13. (bottom, blue) The addition of JDTic largely reversed the observed broadening and chemical shift changes, particularly for residues F4 to R9. (*B*) Overlay of two [^{15}N, ^{1}H]-HSQC-IPAP spectra: (red) KOR + dynorphin and (blue) KOR + dynorphin + JDTic. L5 chemical shift perturbations are mainly in the ^{15}N dimension whereas I8 changes were observed in both ^{1}H and ^{15}N dimensions. The complete spectrum is available in Fig. S4. (*C*) Chemical shift perturbations of dynorphin as a result of KOR binding, calculated as the difference of chemical shifts of dynorphin with KOR and KOR + JDTic. Gray bars (left axis): ^{1}H chemical shifts; white bars (right axis): ^{15}N chemical shifts. The [KOR]/[dynorphin] ratio was 1/100. Almost no chemical shift variations were observed for the C-terminal tripeptide segment.

the weighted average between the bound and free state contributions (33). The σ_{ij} range from 100 to 600 Hz in the bound state and from 0.5 to 3 Hz in the free state and are thus lower than k_{off} for dynorphin–KOR exchange in our experimental conditions. [^{1}H, ^{1}H]-NOESY experiments recorded in the presence and absence of JDTic revealed distinct cross-peak distributions (Fig. 2*A*). NOE build-up curves were obtained from NOESY experiments at four mixing times: 50, 100, 200, and 500 ms. Fig. 2*B* shows a characteristic long-range NOE between the G3α and R6 amide protons. For many resonances, a significant qualitative difference was observed for the build-up rate of NOE intensities with and without JDTic.

The observed NOE build-up differences were thus converted into NMR-derived structural distance restraints using a biexponential fitting routine. Fifty-six significant restraints were used for structure determination (Table 1). Fig. 2*C* qualitatively shows the most significant restraints. Medium- and long-range restraints are clearly concentrated in the central part of the peptide, from F4 to R9. The distance restraints and the R6–R7 dihedral angle restraints were used to determine the structure of dynorphin bound to KOR using a restrained molecular dynamics (MD) protocol as described in *Materials and Methods* and *Supporting Information*. The structure of KOR-bound dynorphin is shown in Fig. 2*D* as an ensemble of 10 best-fit structures derived from the structure determination protocol. In agreement with the restraint table, we found that the central part (from L5 to R9) of the peptide forms a well-defined α-helical turn whereas the N- and C-terminal portions, Y1–F4 and P10–K13, are flexibly disordered.

^{15}N Relaxation Times. Measurement of ^{15}N relaxation rates are routinely applied in protein NMR to characterize internal dynamics. We determined ^{15}N T_1, T_2, and ^{1}H-^{15}N heteronuclear NOEs (hetNOEs) on a peptide ^{15}N-labeled on GFLI residues to assess the peptide dynamics (Fig. S2). Significant variation of the ^{15}N relaxation parameters was observed exclusively for T_2 relaxation times, and thus the related relaxation rate constant R_2. The exclusive variation of R_2 correlates with fast ^{15}N-dynorphin exchange between free and bound states, with a KOR-bound correlation time (τ_c) of 10^{-7} to 10^{-6} s, whereas nonspecifically

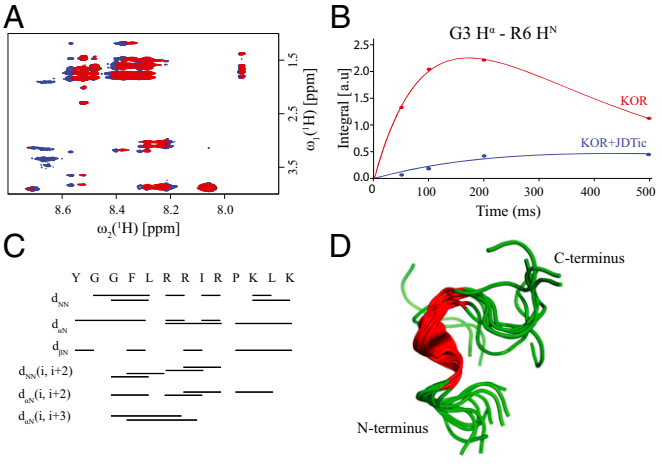

Fig. 2. Structure determination of a KOR-bound conformation of dynorphin. (*A*) Overlay of two 2D [^{1}H, ^{1}H]-NOESY spectra: (red) KOR + dynorphin and (blue) KOR + dynorphin + JDTic; 800 MHz, 100-ms mixing time, 280 K. (*B*) NOE build-up curves for dynorphin cross-peak G3 H^{α}–R6 H^{N} in the presence of (red) KOR and (blue) KOR + JDTic. (*C*) Summary of the most significant NOEs defining the secondary structure. These NOEs are the difference between the observed NOEs in the absence and in the presence of JDTic and are thus representative of KOR specific binding. Note the absence of medium-range NOEs in the N and C termini. (*D*) Conformational ensemble of 10 structures of dynorphin bound to KOR after restrained MD protocols, using the constraints given in Table 1.

Table 1. Statistics for the KOR-bound dynorphin structure determination

No. of restraints for calculations	
Sequential	42
Medium-range (n to n + 2,3,4)	14
Dihedral angles	4
Restraint violations	
NOE restraints, Å	0.07
Coordinate precision: rmsd of backbone atoms, Å	
Residues 1–4	1.76 ± 0.53
Residues 5–8	0.46 ± 0.16
Residues 9–13	5.47 ± 1.92
Residues 1–13	3.57 ± 1.11

Rmsds were computed on the bundle of 10 best conformers used to represent the KOR-bound structure of dynorphin (1–13) (Fig. 2*D*). More detailed statistics and structure validation parameters can be found in Table S2.

bound peptide has a shorter τ_c of 10^{-9} to 10^{-8} s (Fig. S3). ^{15}N T_1 and ^{15}N-^{1}H hetNOEs do not contain significant information on the KOR-bound state (*Materials and Methods* and Figs. S2 and S3). Following these observations, a second set of ^{15}N T_2 relaxation measurements were made on ^{15}N-(GFLI)-,^{15}N,^{13}C-(R)-dynorphin, as shown in Fig. 3*A*.

The difference in R_2 due to KOR binding was recognized as directly proportional to the order parameter, S^2, which describes the amplitude of internal motion of the NH vector (Fig. 3*B*). Changes to R_2 were greater for residues L5–R9 than for G2–F4, and L12 was least affected. In the KOR-bound state, the NH bonds of L5 to R9 are clearly more immobilized than the N and C termini. The ^{1}H-NMR spectrum also indicates the resonances of K11, L12, and K13 were not as broadened by chemical exchange, confirming that these last three residues remain mobile. The internal dynamics of dynorphin are therefore consistent with measured chemical shift perturbations, NOE patterns, and structure in terms of sequence-specific changes. Collectively, these NMR measurements of ^{15}N-dynorphin reflect significant residual mobility in the KOR-bound conformation studied here.

Quantitative analysis of intraresidual NOEs was performed for the side chains of Y1, F4, and P10 where interatomic distances are known. From the initial build-up rates of trNOEs we derived order parameters and found S^2 for F4 was approximately twice that of Y1, and fourfold greater than that of P10. The mobility profile obtained from ^{15}N measurements was thus extended, revealing the phenolic ring of Y1 remains mobile in a KOR-bound state. Interestingly, the F4 aromatic ring is more immobilized than the F4 NH vector (Fig. 3*B*). Similarly, the R9 NH vector has a high S^2 value, whereas the R9 ^{13}C chemical shift indicated the helix is interrupted at the R9 dihedral angles. From the rmsd of the structure determination (Table 1), the helix is defined from L5 to I8, and extends slightly toward F4 (but not its NH) and toward R9 NH (but not its C^{α} or C′ atoms).

Molecular Modeling of KOR–Dynorphin. Starting from the opioid receptor structures 4DJH (KOR), 4N6H (DOR), and 4DKL (MOR), we generated an ensemble of six structures representative of the opioid receptor binding pocket. Flexible docking of dynorphin was performed with a rigid helical turn and MD simulations performed with explicit water (Fig. S5). Five major dynorphin conformations were identified, revealing significant structural diversity in both N and C termini (Table S1; the corresponding pdb files of the peptide receptor complexes are available in Datasets S1–S5). Averaging of NH orientations over five MD simulations, starting from these five poses, in equal proportion, was required to reproduce experimental data.

A comparison of opioid receptor crystal structures provided the basis for interpreting the results from MD. We observed that the position of a phenol-like functional group was largely conserved, in

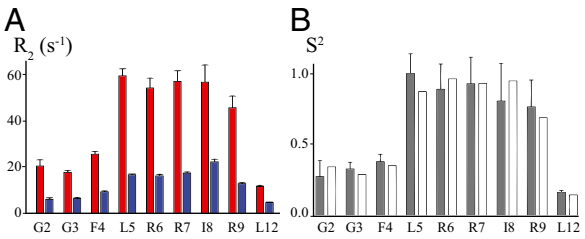

Fig. 3. Characterization of internal dynorphin dynamics. (*A*) ^{15}N R_2 relaxation rate constants (s^{-1}) measured at 600 MHz at 280 K on ^{15}N-(GFLI)-, ^{15}N,^{13}C-(R)-dynorphin in the presence of (red) KOR and (blue) KOR + JDTic. (*B*) (gray) Order parameters profile S^2/S^2_{max} of NH bond vectors derived from R_2 as described in *Supporting Information*. The order parameters describe the amplitude of the NH bond fluctuations in the KOR bound state, normalized to L5. (white) Best-fit S^2 profiles calculated with the ensemble of conformers identified by docking and MD simulations.

terms of position in the orthosteric site, for antagonist-bound structures of KOR-JDTic, DOR-DIPP, and MOR-funaltrexamine (Fig. 4*A*). Following MD simulations the "KOR-1" structural model revealed Y1 in a position near the phenol-piperidine fused-ring system of JDTic, resembling a previously proposed pose (Fig. 4*B*) (9). The "KOR-2" pose of dynorphin placed the Y1 side chain in the sodium allosteric site (Fig. 4*C*). $D^{3.32}$ made polar contacts with Y1, G2, and G3 in both KOR-1 and KOR-2 models, whereas R7 made a polar contact in KOR-2 but not KOR-1. $W^{6.48}$ and $N^{7.45}$ made contacts with Y1 in the KOR-2 model exclusively. Table 2 and Table S1 summarize the findings from modeling and MD simulations, with further details given in *Materials and Methods* and *Supporting Information*.

Discussion

Since the 1970s, pharmacologists and biochemists have attempted to determine opioid peptide conformations capable of explaining their activity and to develop drugs mimicking these conformations (34). In aqueous solutions, peptides often exist as a dynamic ensemble of random coil conformers, with specific folds stabilized by organic solvents or micelles (35–37). Studies of liposome-bound peptides likewise indicate that nonpolar or membrane-like environments stabilize peptide structure (23, 24, 38–41). Schwyzer introduced the "membrane compartment concept" that postulated the membrane-bound state as part of the binding mechanism, thereby reducing the available peptide conformations toward an activating conformation in complex with receptor (21, 22, 25). For many years, the direct analysis of the peptide–receptor complex was not possible due to the lack of suitable receptor preparations. Recently, several neurotensin–receptor complexes have been studied both by X-ray crystallography and solid-state NMR (11–13), and the structure of the Leukotriene B4 (a proinflammatory lipid mediator), in complex with the human BLT2 receptor, was determined by liquid-state NMR (41).

Recent advances in producing the opioid receptors (and other GPCRs) in milligram quantities via transient insect cell expression and stabilization in a bicelle-like architecture of mixed detergent-sterol micelles has opened new avenues for opioid receptor structural biology (42). This progress culminated in 2012, with reports of inactive state structures determined by X-ray crystallography of the four opioid receptors in complex with antagonists or inverse agonists (10, 43–46). Currently, the only reported 3D structure of the human KOR is in complex with JDTic, a highly potent KOR antagonist.

NMR using (^{15}N-^{13}C)–labeled ligand represents a powerful complementary alternative to crystallographic approaches in obtaining structural information of receptor activation by peptide agonists. Owing to the moderate affinity of dynorphin with KOR reconstituted in detergent micelles and fast association rate, the ligand dissociation rate is also fast on the NMR chemical shift time scale (47). This context made possible the observation of trNOEs and a straightforward interpretation of ^{15}N relaxation rates (33). The receptor–peptide interaction was therefore ideal to determine a KOR-bound conformation of dynorphin via the trNOE method, as well as to characterize internal peptide dynamics in a bound state. Such an approach would be prohibited in a comparable study of the high-affinity state, which is characterized by low nanomolar K_d and longer off-rate. In this case, changes to dynorphin structure and dynamics are expected as a result of G protein binding to KOR. Nevertheless, NMR observation of the high-affinity state of dynorphin can be pursued by deuteration of the receptor, peptide, and cognate inhibitory G proteins and preparation of a 1:1:1 complex at millimolar concentrations.

The computational approaches were insufficient to determine reasonable models of dynorphin–KOR binding, because multiple conformers of similar energy were observed. The NMR observations of structure and dynamics were required to limit the starting poses of dynorphin for MD. We identified the pose KOR-1 as typical of an inactive state based on the proximity of Y1 to the phenol-like functional group of JDTic (Fig. 4*B* and Fig. S6*B*). In contrast, we speculate the conformational change of the peptide found in KOR-2 correlates with an activated state (Fig. 4 *B* and *C* and Fig. S6*D*). The position of Y1 in the KOR-2 model corresponds with an established role in activation, with the dynorphin (2–13) peptide previously reported to bind weakly and not activate KOR (48). In this "active" conformation, the N terminus of dynorphin forms polar interactions with $N^{3.35}$ and $D^{3.32}$ side chains, whereas the Y1 phenol ring is involved in a π-stacking interaction with $W^{6.48}$ and an H-bond with $N^{7.45}$. As part of the allosteric sodium site these residues stabilize an inactive state of the receptor, with changes to dynorphin structure providing agonist–receptor contacts among highly conserved residues in transmembrane helices 6 and 7 (43). Interestingly, this conformational change may be associated with an

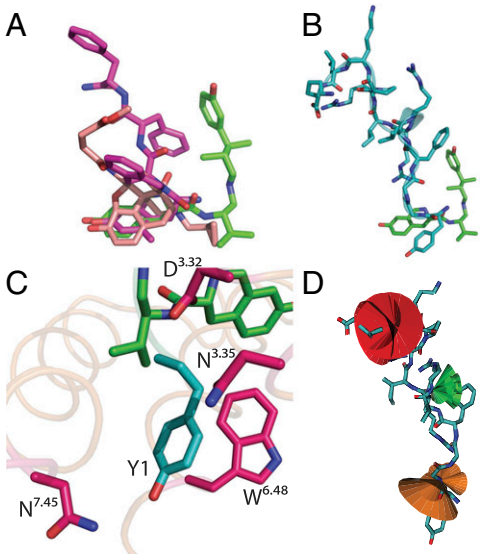

Fig. 4. Ligand poses from modeling the dynorphin–KOR complex. (*A*) Antagonist binding poses from structures of KOR-JDTic (4DJH), DOR-DIPP (4RWA), and MOR-FNA (4DKL). JDTic is shown in green, DIPP in purple, and β-funaltrexamine in salmon. (*B*) Structure of dynorphin in complex with "KOR-1" from MD simulations with Y1 in a position near the fused phenol-piperidine ring system of JDTic. (*C*) Zoom on dynorphin Y1 in the "KOR-2" complex. Y1 is positioned toward the sodium allosteric binding site. Dynorphin–KOR contacts are given in Table 2 and Table S1. (*D*) Visual representation of order parameters derived from NMR relaxation measurements. The width of the cone indicates the flexibility of G2 (orange), R6 (green), and L12 (red) dynorphin residues in a KOR-bound state.

Table 2. Most important contacts between dynorphin and KOR

Dynorphin	KOR-1	KOR-2
Interaction energy	−22.68 kcal·mol^{-1}	−21.11 kcal·mol^{-1}
Tyr1	Asp138 (3.32)	Asp138 (3.32)
	Met142 (3.36)	Asn141 (3.35)
	Val230 (5.42)	Asn322 (7.45)
		Trp287 (6.48)
Gly2	Asp138 (3.32)	Asp138 (3.32)
	Tyr139 (3.33)	
Gly3	Asp138 (3.32)	Asp138 (3.32)
Arg6		Glu209
Arg7	Asp223 (5.35)	Asp138 (3.32)
	Met226 (5.38)	

The receptor contacts are shown with Ballesteros and Weinstein numberings for helical residues in parentheses (63). A more detailed list of contacts for the five major conformations of dynorphin is provided in Table S1. The interaction energies were computed using contacts of dynorphin 1–8 residues.

increased penetration of water into the receptor cavity, which has been linked to the activation mechanism upon agonist binding (49). Mutations of the sodium site in DOR shift nalfurafine, an antagonist, to an arrestin-biased ligand, establishing this sodium site as a key mediator of receptor function (43). The KOR-2 conformation may hint at the mechanism of dynorphin functional selectivity, which has been reported as a G protein-biased agonist in pharmacological in vitro studies (50, 51). The proposed model may be tested in future studies by mutagenesis of KOR residues that surround dynorphin in the KOR-2 conformation.

The direct quantification of neuropeptide dynamics in an intermediate-affinity receptor-bound state yields useful insights for the design of KOR-targeting antagonists as well as the biology of peptide-activated receptors. More surprising than the well-defined α-helical turn between L5 and R9 was the significant motion observed for the N and C termini. Such motion was expected for the C-terminal part of dynorphin: Indeed, within the message–address paradigm the highly positively charged C-terminal "address" is expected to produce favorable but nonspecific electrostatic interactions with the negatively charged extracellular loop 2. In contrast, this mobility was entirely unexpected for the first four residues YGGF known to be crucial for the activation of opioid receptors and form the so-called "message" part of the peptide.

The biology of peptide agonists may also be reflected in flexibly disordered N and C termini in a bound, but not activating, state. It is feasible that a combination of attractive and repulsive forces have been selected for through evolution so that peptide agonists do not remain bound for excessively long periods, allowing enkephalinases to degrade potent bioactive neuropeptides (52). Whereas GPCRs exist in an array of states with variable ligand affinity, the observations of dynorphin in complex with KOR indicate that there are multiple bound states of the peptide that correspond with various ensembles of activated receptor. We postulate that the KOR-bound conformation reported here, retaining a significant degree of freedom, reflects the mechanism of receptor binding and activation. It would involve, in an initial stage, the association of helix L5 to R9 into the binding pocket and, in a second stage, the conversion of the receptor into the active conformation concomitant with structural immobilization of the N-terminal "message" part of the peptide.

Materials and Methods

Peptide Synthesis. Peptide synthesis was performed using standard solid-phase synthesis as described in *Supporting Information*.

KOR Expression, Purification, and Reconstitution in Detergent Micelles. KOR samples were prepared as previously published and described in *Supporting Information* (10).

NMR Experiments. The NMR data were measured at 280 K on a Bruker Avance III 800 MHz for the ^{15}N-(GFLI)–labeled dynorphin and on a Bruker Avance III 600 MHz for the ^{15}N(GFLI)- and ^{15}N-^{13}C(R)–labeled dynorphin. The peptide was dissolved to 1 mM in a buffer containing 40 mM deuterated MES (Mes_d), pH 6.1, 150 mM KCl, 100 μM 2,2 dimethyl-2-silapentane-5-sulfonic acid (DSS), and 10% D_2O for frequency lock. To a 1 mM peptide solution was added KOR reconstituted in detergent micelles to a final concentration of 10 μM, a 1:100 ratio of receptor to ligand. The concentration of DDM was 8 mM and CHS 1.6 mM, respectively, as measured by ^{1}H-NMR. Standard 1D ^{1}H, 1D ^{13}C, 2D [^{1}H, ^{1}H]-TOCSY, and NOESY experiments were acquired using excitation sculpting for water suppression (53–55). [^{15}N, ^{1}H]-HSQC, [^{13}C, ^{1}H]-HSQC, [^{15}N, ^{1}H]-IPAP-HSQC, and CBCANH pulse programs were used to perform the ^{1}H, ^{15}N and ^{13}C-Arg assignments of dynorphin in aqueous solvent, with KOR, and with KOR and JDTic (30, 56–58). The assignments were obtained using the standard reported strategy for ^{1}H, with ^{15}N and ^{13}C assignments transferred to heteronuclear correlation experiments based on ^{1}H assignments (28). The ^{1}H, ^{15}N, and ^{13}C assignments of the free peptide have been deposited in the BMRB (accession no. 25597).

NOESY experiments were acquired at four mixing times: 50, 100, 200, and 500 ms to generate build-up curves. ^{15}N relaxation rates, R_1 (inversion recovery), R_2 (CPMG), and ^{1}H-^{15}N hetNOEs were measured with established experiments (59). After data acquisition in the presence of KOR, JDTic was added to a final concentration of 1 mM and the complete set of NMR experiments was performed again to report on the nonspecific binding of dynorphin.

Structure Determination. Direct comparison of NOE spectra were normalized in the following manner. NOE volumes in spectra with and without JDTic were integrated for all mixing times. The integrals were rescaled to take into account the interactions between groups of equivalent spins. The build-up curves were fitted to a biexponential analytic function, which permitted estimation of the cross-relaxation rates. The NOEs in the bound state were calculated assuming a weighted average of the free and bound states, with weights equal to populations in both states. Finally, the NOEs were calibrated with respect to the H^N-H^α peaks from the backbone of the peptide. The initial set of NOEs contained 105 peaks, from which 22 indirect NOEs were eliminated, characterized by sigmoidal build-up curves, as well as 20 NOEs with uncertain integrals due to peak overlap. The intraresidual H^N-H^α NOEs were used only for calibration. Hence, in total, 56 NOEs and 4 dihedral angle restraints (for R6 and R7 dihedral angles) were used for the structure determination (Table 1). Further details of the structure determination protocol are given in Table S2. The ensemble of 10 best structures have been deposited in the Protein Data Bank (ID code 2N2F).

^{15}N Relaxation Rates. Relaxation rates were analyzed using the standard equations described by Farrow (59). In conditions of fast exchange between three states, namely receptor-bound, nonspecific binding, and the free peptide in solution, relaxation parameters were measured as a weighted average of their respective values in each state (60). Owing to the R_1 and hetNOE dependence on rotational diffusion correlation times (Fig. S3), it is academic to establish R_1 and hetNOE should not be significantly affected by the small fraction of bound receptor, whereas the R_2 contribution arising from the bound fraction is proportional to the NH order parameters in the bound state (*Supporting Information*).

Molecular Modeling of KOR–Dynorphin Complexes. Details of the molecular modeling protocols are given in *Supporting Information* and briefly summarized here. We started from the 3D structure of KOR-JDTic published in 2012 (9). Because JDTic induces certain conformational changes by disrupting the salt bridge involving Gln115, Asp138, and Tyr320, we mutated the known structure of MOR into KOR (45). Missing side chains were added and optimized using the SCWRL4 software (61). Out of thousands of possible poses, 10 poses per structure were retained based on a combination of (*i*) docking score, (*ii*) interaction of the positively charged C terminus with the negatively charged extracellular loops, and (*iii*) the competitive binding with JDTic. Each of these poses was then submitted to a 50-ns MD simulation in explicit water. The equilibrated parts of the trajectories (the last 20 ns) were used for subsequent analyses.

The energies of intermolecular interaction between dynorphin and KOR were determined using the MMPBSA method (62). The flexibility of the C terminus on the nanosecond scale was clearly demonstrated in MD simulations (Fig. S4). In contrast, the N terminus is fairly rigid in each simulation, with the existence of distinct starting conformations consistent with reorientations on a slower time scale. The interconversion between these conformations was still not observed after a 1-μs MD simulation performed on KOR-2, with NMR restraints required fixing the central helix. The MD runs were performed over 50 ns in a periodic box with explicit solvent, including four water molecules present in crystal structures of KOR, DOR, and MOR, and with ions neutralizing the charges of the system. The equilibrated parts of the trajectories have been subject to detailed analysis.

ACKNOWLEDGMENTS. We thank G.J. Kroon and O. Saurel for help in acquiring ^{15}N relaxation data, H. Mazarguil for help with peptide synthesis and purification, and A. Walker for final edits. University Paul Sabatier Toulouse allowed A. Milon to spend a sabbatical semester at The Scripps Research Institute. This work was supported by National Institutes of Health/National Institute of General Medical Sciences Roadmap Initiative for Structural Biology Grant P50 GM073197, Protein Structure Initiative (PSI-Biology) Grant U54 GM094618, and National Institute of Drug Abuse Project Grant P01 DA035764 for Structure-Function of Opioid Receptors. K.W. is the Cecil H. and Ida M. Green Professor of Structural Biology at The Scripps Research Institute.

1. Katritch V, Cherezov V, Stevens RC (2012) Diversity and modularity of G protein-coupled receptor structures. *Trends Pharmacol Sci* 33(1):17–27.
2. Katritch V, et al. (2014) Allosteric sodium in class A GPCR signaling. *Trends Biochem Sci* 39(5):233–244.
3. Katritch V, Cherezov V, Stevens RC (2013) Structure-function of the G protein-coupled receptor superfamily. *Annu Rev Pharmacol Toxicol* 53:531–556.
4. Liu JJ, Horst R, Katritch V, Stevens RC, Wüthrich K (2012) Biased signaling pathways in β2-adrenergic receptor characterized by 19F-NMR. *Science* 335(6072):1106–1110.
5. Kofuku Y, et al. (2014) Functional dynamics of deuterated β2 -adrenergic receptor in lipid bilayers revealed by NMR spectroscopy. *Angew Chem Int Ed Engl* 53(49):13376–13379.
6. Manglik A, et al. (2015) Structural insights into the dynamic process of β2-adrenergic receptor signaling. *Cell* 161(5):1101–1111.
7. Pasternak GW (2014) Opioids and their receptors: Are we there yet? *Neuropharmacology* 76(Pt B):198–203.
8. Carroll FI, Carlezon WA, Jr (2013) Development of κ opioid receptor antagonists. *J Med Chem* 56(6):2178–2195.
9. Vardy E, et al. (2013) Chemotype-selective modes of action of κ-opioid receptor agonists. *J Biol Chem* 288(48):34470–34483.
10. Wu H, et al. (2012) Structure of the human κ-opioid receptor in complex with JDTic. *Nature* 485(7398):327–332.
11. Luca S, et al. (2003) The conformation of neurotensin bound to its G protein-coupled receptor. *Proc Natl Acad Sci USA* 100(19):10706–10711.
12. White JF, et al. (2012) Structure of the agonist-bound neurotensin receptor. *Nature* 490(7421):508–513.
13. Egloff P, et al. (2014) Structure of signaling-competent neurotensin receptor 1 obtained by directed evolution in Escherichia coli. *Proc Natl Acad Sci USA* 111(6): E655–E662.
14. Chavkin C, Goldstein A (1981) Specific receptor for the opioid peptide dynorphin: Structure–activity relationships. *Proc Natl Acad Sci USA* 78(10):6543–6547.
15. Chavkin C, Goldstein A (1981) Demonstration of a specific dynorphin receptor in guinea pig ileum myenteric plexus. *Nature* 291(5816):591–593.
16. Chavkin C, Bakhit C, Weber E, Bloom FE (1983) Relative contents and concomitant release of prodynorphin/neoendorphin-derived peptides in rat hippocampus. *Proc Natl Acad Sci USA* 80(24):7669–7673.
17. Oka T, et al. (1982) Evidence that dynorphin-(1-13) acts as an agonist on opioid kappa-receptors. *Eur J Pharmacol* 77(2-3):137–141.
18. Roth BL, et al. (2002) Salvinorin A: A potent naturally occurring nonnitrogenous kappa opioid selective agonist. *Proc Natl Acad Sci USA* 99(18):11934–11939.
19. Tao YM, et al. (2008) LPK-26, a novel kappa-opioid receptor agonist with potent antinociceptive effects and low dependence potential. *Eur J Pharmacol* 584(2-3):306–311.
20. White KL, et al. (2015) The G protein-biased κ-opioid receptor agonist RB-64 is analgesic with a unique spectrum of activities in vivo. *J Pharmacol Exp Ther* 352(1):98–109.
21. Schwyzer R (1986) Estimated conformation, orientation, and accumulation of dynorphin A-(1-13)-tridecapeptide on the surface of neutral lipid membranes. *Biochemistry* 25(15): 4281–4286.
22. Sargent DF, Schwyzer R (1986) Membrane lipid phase as catalyst for peptide-receptor interactions. *Proc Natl Acad Sci USA* 83(16):5774–5778.
23. Björnerås J, et al. (2014) Direct detection of neuropeptide dynorphin A binding to the second extracellular loop of the κ opioid receptor using a soluble protein scaffold. *FEBS J* 281(3):814–824.
24. Zhang L, DeHaven RN, Goodman M (2002) NMR and modeling studies of a synthetic extracellular loop II of the kappa opioid receptor in a DPC micelle. *Biochemistry* 41(1):61–68.
25. Erne D, Sargent DF, Schwyzer R (1985) Preferred conformation, orientation, and accumulation of dynorphin A-(1-13)-tridecapeptide on the surface of neutral lipid membranes. *Biochemistry* 24(16):4261–4263.
26. Portoghese PS (1989) Bivalent ligands and the message-address concept in the design of selective opioid receptor antagonists. *Trends Pharmacol Sci* 10(6):230–235.
27. Nygaard R, et al. (2013) The dynamic process of β(2)-adrenergic receptor activation. *Cell* 152(3):532–542.
28. Wüthrich K (1986) *NMR of Proteins and Nucleic Acids* (Wiley, New York).
29. Ulrich EL, et al. (2008) BioMagResBank. *Nucleic Acids Res* 36(Database issue):D402–D408.
30. Ottiger M, Delaglio F, Bax A (1998) Measurement of J and dipolar couplings from simplified two-dimensional NMR spectra. *J Magn Reson* 131(2):373–378.
31. Wishart DS (2011) Interpreting protein chemical shift data. *Prog Nucl Magn Reson Spectrosc* 58(1-2):62–87.
32. Costello GF, Main BG, Barlow JJ, Carroll JA, Shaw JS (1988) A novel series of potent and selective agonists at the opioid kappa-receptor. *Eur J Pharmacol* 151(3):475–478.
33. Clore GM, Gronenborn AM (1983) Theory of the time-dependent transferred nuclear Overhauser effect: Applications to structural analysis of ligand–protein complexes in solution. *J Magn Reson* 53(3):423–442.
34. Roques BP, Garbay-Jaureguiberry C, Oberlin R, Anteunis M, Lala AK (1976) Conformation of Met5-enkephalin determined by high field PMR spectroscopy. *Nature* 262(5571):778–779.
35. Lancaster CR, et al. (1991) Mimicking the membrane-mediated conformation of dynorphin A-(1-13)-peptide: Circular dichroism and nuclear magnetic resonance studies in methanolic solution. *Biochemistry* 30(19):4715–4726.
36. Spadaccini R, Crescenzi O, Picone D, Tancredi T, Temussi PA (1999) Solution structure of dynorphin A (1-17): A NMR study in a cryoprotective solvent mixture at 278 K. *J Pept Sci* 5(7):306–312.
37. Naito A, Nishimura K (2004) Conformational analysis of opioid peptides in the solid states and the membrane environments by NMR spectroscopy. *Curr Top Med Chem* 4(1):135–145.
38. Milon A, Miyazawa T, Higashijima T (1990) Transferred nuclear Overhauser effect analyses of membrane-bound enkephalin analogues by 1H nuclear magnetic resonance: correlation between activities and membrane-bound conformations. *Biochemistry* 29(1):65–75.
39. Augé S, Bersch B, Tropis M, Milon A (2000) Characterization of substance P-membrane interaction by transferred nuclear Overhauser effect. *Biopolymers* 54(5):297–306.
40. Lind J, Gräslund A, Mäler L (2006) Membrane interactions of dynorphins. *Biochemistry* 45(51):15931–15940.
41. Catoire LJ, et al. (2010) Structure of a GPCR ligand in its receptor-bound state: leukotriene B4 adopts a highly constrained conformation when associated to human BLT2. *J Am Chem Soc* 132(26):9049–9057.
42. Thompson AA, et al. (2011) GPCR stabilization using the bicelle-like architecture of mixed sterol-detergent micelles. *Methods* 55(4):310–317.
43. Fenalti G, et al. (2014) Molecular control of δ-opioid receptor signalling. *Nature* 506(7487):191–196.
44. Granier S, et al. (2012) Structure of the δ-opioid receptor bound to naltrindole. *Nature* 485(7398):400–404.
45. Manglik A, et al. (2012) Crystal structure of the μ-opioid receptor bound to a morphinan antagonist. *Nature* 485(7398):321–326.
46. Thompson AA, et al. (2012) Structure of the nociceptin/orphanin FQ receptor in complex with a peptide mimetic. *Nature* 485(7398):395–399.
47. Catoire LJ, Damian M, Baaden M, Guittet E, Banères JL (2011) Electrostatically-driven fast association and perdeuteration allow detection of transferred cross-relaxation for G protein-coupled receptor ligands with equilibrium dissociation constants in the high-to-low nanomolar range. *J Biomol NMR* 50(3):191–195.
48. Lai J, et al. (2006) Dynorphin A activates bradykinin receptors to maintain neuropathic pain. *Nat Neurosci* 9(12):1534–1540.
49. Yuan S, et al. (2015) The mechanism of ligand-induced activation or inhibition of μ- and κ-opioid receptors. *Angew Chem Int Ed Engl* 54(26):7560–7563.
50. Bruchas MR, et al. (2007) Stress-induced p38 mitogen-activated protein kinase activation mediates kappa-opioid-dependent dysphoria. *J Neurosci* 27(43):11614–11623.
51. White KL, et al. (2014) Identification of novel functionally selective κ-opioid receptor scaffolds. *Mol Pharmacol* 85(1):83–90.
52. Gorenstein C, Snyder SH (1980) Enkephalinases. *Proc R Soc Lond B Biol Sci* 210(1178): 123–132.
53. Piotto M, Saudek V, Sklenár V (1992) Gradient-tailored excitation for single-quantum NMR spectroscopy of aqueous solutions. *J Biomol NMR* 2(6):661–665.
54. Shaka AJ, Lee CJ, Pines A (1988) Iterative schemes for bilinear operators; Application to spin decoupling. *J Magn Reson* 77(2):274–293.
55. Hwang TL, Shaka AJ (1995) Water suppression that works. Excitation sculpting using arbitrary wave-forms and pulsed-field gradients. *J Magn Reson A* 112(2):275–279.
56. Sklenar V, Piotto M, Leppik R, Saudek V (1993) Gradient-tailored water suppression for H-1-N-15 Hsqc experiments optimized to retain full sensitivity. *J Magn Reson A* 102(2):241–245.
57. Vuister GW, Bax A (1992) Resolution enhancement and spectral editing of uniformly C-13-enriched proteins by homonuclear broad-band C-13 decoupling. *J Magn Reson* 98(2): 428–435.
58. Grzesiek S, Bax A (1992) An efficient experiment for sequential backbone assignment of medium-sized isotopically enriched proteins. *J Magn Reson* 99(1):201–207.
59. Farrow NA, et al. (1994) Backbone dynamics of a free and phosphopeptide-complexed Src homology 2 domain studied by 15N NMR relaxation. *Biochemistry* 33(19):5984–6003.
60. Woessner DE (1996) Relaxation effects of chemical exchange. *Encyclopedia of NMR*, eds Grant DM, Harris RK (Wiley, New York), Vol 6.
61. Krivov GG, Shapovalov MV, Dunbrack RL, Jr (2009) Improved prediction of protein side-chain conformations with SCWRL4. *Proteins* 77(4):778–795.
62. Miller BR, et al. (2012) MMPBSA.py: An efficient program for end-state free energy calculations. *J Chem Theory Comput* 8(9):3314–3321.
63. Ballesteros JA, Weinstein H (1995) Integrated methods for the construction of three dimensional models and computational probing of structure–function relations in G-protein coupled receptors. *Methods Neurosci* 25:366–428.
64. Fersht AR (1999) *Structure and Mechanism in Protein Science* (Freeman, New York).
65. Axelrod D, Wang MD (1994) Reduction-of-dimensionality kinetics at reaction-limited cell surface receptors. *Biophys J* 66(3 Pt 1):588–600.
66. Arai M, Ferreon JC, Wright PE (2012) Quantitative analysis of multisite protein-ligand interactions by NMR: Binding of intrinsically disordered p53 transactivation subdomains with the TAZ2 domain of CBP. *J Am Chem Soc* 134(8):3792–3803.
67. Salomon-Ferrer R, Case DA, Walker RC (2013) An overview of the Amber biomolecular simulation package. *WIREs Comput Mol Sci* 3(2):198–210.